



ORIGINAL RESEARCH ARTICLE

Experimental Study on Microbial Activity of Ship Ballast Water and Corrosion of Ballast Tank by Inert Flue Gas Deoxidation

Jun Wang, Ruoxi Ding , Junxia Li, Yaohui Liu, and Ning Chen

Submitted: 8 October 2022 / Revised: 7 February 2023 / Accepted: 22 December 2023

To explore how to reduce the corrosion of ship ballast tanks while killing planktonic microorganisms in ship ballast water and meeting the prescribed ballast water discharge standards, an experimental system for inert flue gas pressure-loaded water treatment was established in this paper. The simulated seawater was treated with the combined inert flue gas of N_2 and CO_2 , and the corrosion weight loss of the ballast tank steel plate samples in different corrosive media was simulated. The results showed that when the dissolved oxygen concentration in the ballast water was 0.5 mg/L and the pH value was 6, the mortality of *Chlorella* reached 100%, the mortality of *Escherichia coli* was 99.98%, and the microbial lethality met the D-2 standard. The average corrosion rate of the samples in the corrosive medium with an oxygen concentration of 0.5 mg/L and a pH of 6 was 69.02% lower than the average corrosion rate of the samples in simulated seawater. The results were consistent with the results calculated by the weight loss method, which indicated that the use of the inert flue gas deoxygenation method to treat the ship's ballast water reduced the corrosion rate of the ballast tanks.

Keywords ballast tank corrosion, ballast water treatment, inert flue gas, microorganism

1. Introduction

The damage of marine species in the marine environment caused by ship ballast water has been identified as one of the four major threats to oceans by the Global Environment Fund (GEF). Ships transport more than 80% of the world's commodities, and approximately 10 billion tons of ballast water is transferred globally each year. Approximately 3000 species of animals and plants migrate around the world through ballast water every day, causing serious damage to the natural ecological environment. In 2004, the International Maritime Organization (IMO) adopted the "International Convention on the Control and Management of Ships' Ballast Water and Sediments," aiming to reach an international consensus "to prevent, reduce and ultimately eliminate the spread of harmful aquatic organisms and pathogens."

At present, there are at least 30 treatment methods for ship ballast water in the world, mainly including physical, chemical and biological treatment (Ref 1-3). Ballast water treatment methods such as filtration, deoxidation, ultraviolet treatment and ultrasonic waves follow G8 guidelines, while treatment methods such as electrolysis, ozone and organic biocides follow

G9 guidelines (Ref 4, 5). A large number of experimental studies have shown that these methods are successful, but there are some shortcomings in practical applications.

Scholars have proposed the deoxygenation method to treat ballast water and studied its effect on killing planktonic microorganisms with certain positive results. In 2002, Tamburria (Ref 6) found that the removal of oxygen from ballast tanks by the nitrogen deoxygenation method could significantly kill some aerobic bacteria and reduce the corrosion of ships. At the same time, a number of facultative anaerobic species were able to multiply in deoxygenated ballast water; in 2007, McCollin et al. (Ref 7) investigated bacterial growth by adding nutrients to a ballast tank. The results of their study found that after 5 days, the number of surviving zooplankton in the ballast tank decreased sharply, but the killing effect on obligate anaerobic bacteria and phytoplankton was not obvious. In 2008, Xiao et al. (Ref 8) studied the effect of nitrogen on the growth of plankton in ship ballast water. The results showed that the inert gas protective layer formed by nitrogen could significantly inhibit and partially inhibit the growth of organisms in ballast water. The lethal effect of nitrogen filling improved the effect of electrolysis to treat ship ballast water. In 2008, Zhou et al. (Ref 9) discussed the use of an inert gas to replace air in the ballast system of ocean-going ships so that the dissolved oxygen in the water was less than 1 mg/l, which would suffocate aquatic organisms. In 2012, Ma (Ref 10) discussed the use of an inert gas generation and delivery system as a method to treat ship ballast water with relative economy and effectiveness. In 2012, Huang (Ref 11) conducted a study on the Venturi deoxygenation method for the treatment of ship ballast water. The study showed that the seawater treated by this method met the ballast water discharge standards stipulated in the convention and was energy-saving, environmentally friendly, and easy to use.

Jun Wang, Ruoxi Ding, Junxia Li, Yaohui Liu, and Ning Chen, School of Energy and Power Engineering, Jiangsu University of Science and Technology, Zhenjiang 212003, China. Contact e-mail: dingxi322@163.com.

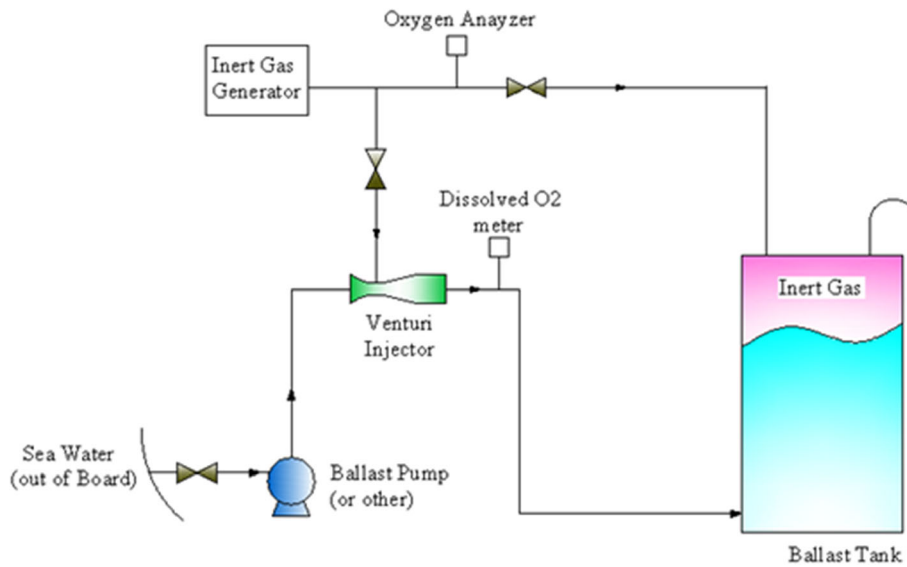


Fig. 1 Flowchart of the VOS system

Taking NEI's Venturi deoxygenation ballast water treatment system (Venturi Oxygen Stripping—VOS) as an example, the working principle of the system is illustrated. This technology has been proven in ship experiments and fully complies with the IMO ballast water discharge standards (Ref 12). Figure 1 shows the flowchart of the VOS system.

The VOS system is combined with the existing ballast system of the ship. When the ballast water flows through the Venturi injector installed on the ballast pipeline, cavitation occurs. It is supersaturated with nitrogen. After this process, the oxygen content in the ballast water is reduced by 95% within 10 sec. When the ballast water is discharged from the ballast tank, the VOS system injects nitrogen into a void through the deck pipeline to maintain a low-oxygen environment in the ballast tank and prevent the formation of iron oxide or rust; at the same time, the low-oxygen environment greatly reduces the survival rate of aquatic organisms brought with ballast water (Ref 13, 14).

During the voyage of the ship, accompanied by a large amount of flue gas emissions, after the flue gas undergoes desulfurization and denitration treatment, the oxygen content of the flue gas is generally less than 0.5 mg/L, which is a good inert flue gas (mainly including N₂, CO₂ and a small amount of O₂). The use of this inert flue gas to treat ballast water can achieve resource reuse (Ref 15-17).

In this study, the exhaust gas of a marine diesel engine was simulated, the ship's ballast water was treated by the deoxygenation method, and an experimental system was constructed.

2. Study on Inactivation of Microorganisms by Inert Flue Gas

When inert flue gas is used to treat ballast water, the properties of seawater change after inert flue gas is introduced into the ballast tank, which changes the environment and affects the growth of microorganisms.

2.1 Mechanism of the Inert Flue Gas Deoxidation Method

Inert flue gas is mainly composed of N₂ and CO₂ and small amounts of O₂ and other gas components. According to Henry's law and Dalton's law of partial pressure, and

$$P_g = Hx \quad (\text{Eq 1})$$

where H is Henry's constant, X is the mole fraction solubility of a gas, and P_g is the partial pressure of a gas.

$$p = \sum_{i=1} p_i \quad p_i = y_i p \quad (\text{Eq 2})$$

where p is the gas pressure above the liquid and p_i is the partial pressure of the gas above the liquid.

From Henry's law and Dalton's law of partial pressure, the gas-liquid two-phase equilibrium equation of the ballast tank after inert flue gas treatment can be obtained, as shown in Eq 3 and 4.

$$P_2^* + P_3^* = H_2 X_2 + H_3 X_3 \quad (\text{Eq 3})$$

$$y_2 p + y_3 p = H_2 X_2 + H_3 X_3 \quad (\text{Eq 4})$$

where P_2^* is the partial pressure of oxygen and P_3^* is the partial pressure of inert flue gas. y_2 and y_3 are the gas-phase mole fractions of oxygen and inert flue gas, respectively. The solubilities of oxygen and inert gases in water are small, and Eq 5 and 6 are obtained from the simplified formula of the phase equilibrium formula:

$$(m_2 X_2 + m_3 X_3) p = H_2 X_2 + H_3 X_3 \quad (\text{Eq 5})$$

$$X_2 = - \left(\frac{m_3 p - H_3}{m_2 p - H_2} \right) X_3 \quad (\text{Eq 6})$$

where m_2 and m_3 are the phase equilibrium constants of oxygen and inert flue gas. As can be seen from Eq (3)-(6), the solubility of oxygen in water is also affected by the total pressure above the liquid. When the pressure is small, the

solubility of oxygen in the ballast water does not change much. When the pressure reaches a certain value, the higher the pressure, the smaller the dissolved oxygen concentration.

Based on the above two laws, when the ship is ballasted, inert flue gas is injected. First, the inert flue gas passes through the ejector to form a certain number of air pockets in the ballast water. During the upward movement of the air pockets, it absorbs some of the dissolved oxygen in the ballast water. Second, as the volume of ballast water in the ballast tank increases, the air in the tank is compressed to make its pressure greater than that of the outside atmosphere, and thus the residual air in the ballast tank is discharged into the atmosphere through the breathing valve of the ballast tank ventilation pipe, and continues. Filled with inert flue gas, its partial pressure has an absolute advantage, and the dissolved oxygen dissolved in the ballast water is driven out. In the case of keeping the ballast tank closed under the positive pressure, the inert flue gas always has an advantage, and the very small amount of free oxygen in the air space of the ballast tank cannot be dissolved in the ballast water, thereby driving the dissolved oxygen from the ballast water.

2.2 Inert Flue Gas Affects the Microbial Reaction Mechanism

The inert flue gas affects the microbial reaction mechanism mainly through environmental factors that affect the microbial reaction. When inert flue gas is introduced into ballast water, it mainly changes the dissolved oxygen concentration and pH value of the ballast water.

- (1) The effect of dissolved oxygen on microbial responses: The utilization of oxygen by microorganisms depends on the solubility of oxygen in the solution and the rate of oxygen transfer. Mass transfer during microbial growth is very complex and related to oxygen partial pressure and concentration. According to double-membrane theory, changes in oxygen partial pressure and concentration near the gas-liquid interface are shown in Fig. 2. For the oxygen transfer rate, the liquid phase concentration is used as a reference, as shown in Eq 7;

$$N = \frac{\text{Driving force}}{\text{Resistance}} = \frac{c_i - c}{1/k_L} = \frac{c^* - c}{1/k_G} = \frac{c^* - c}{1/k_L + H/k_G} = K_L(c^* - c) \quad (\text{Eq 7})$$

where k_L is the liquid film mass transfer coefficient, k_G is the gas film mass transfer coefficient, c_i is the equilibrium concentration at the gas-liquid interface, c is the oxygen concentration in the main stream of solution, c^* is the oxygen concentration in equilibrium at the gas-phase oxygen partial pressure, H is Henry's constant, and K_L is the total mass transfer coefficient based on a liquid film. The magnitude of each mass transfer resistance depends on the solubility of the gas. If the solubility of the gas in the liquid phase is high, then the mass transfer resistance of the liquid phase is negligible relative to that of the gas phase; in contrast, for a gas with low solubility, the total mass transfer coefficient K_L is close to the liquid film mass transfer coefficient k_L . The mass process is controlled by the transport process in the liquid phase.

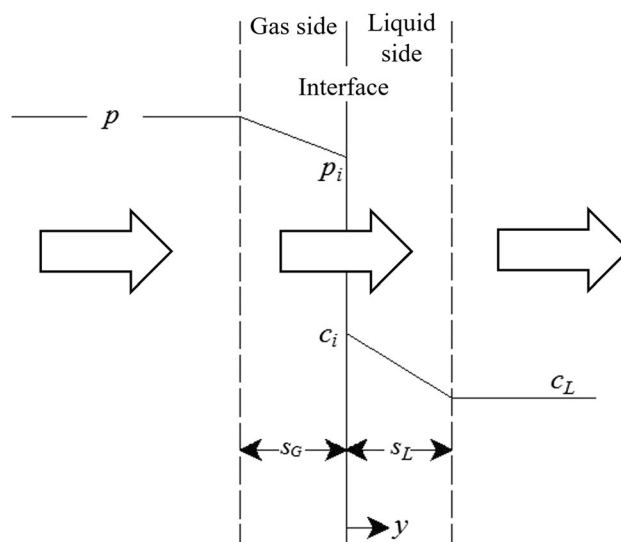


Fig. 2 Double-membrane theoretical model for oxygen transfer near the gas-liquid interface

- (2) Influence of pH value on microbial reaction: Different microorganisms have their own optimum pH range for growth and microbial reactions. The pH of most natural environments is between 5 and 9, and the optimum growth pH for many microorganisms is also within this range. Only a few species can grow in environments with pH values below 2 or above 10. The optimum pH for most bacteria, algae and protozoa is 6.5-7.5.

2.3 Corrosion Mechanism of Ballast Water on Ballast Tanks After Inert Flue Gas Treatment

When inert flue gas is used to treat ballast water, inert flue gas is introduced into the ballast tank, the properties of seawater change, and the ballast tank is in a new corrosion system.

2.3.1 Factors Affecting Metal Corrosion in Seawater. The factors that affect the corrosion of metals in seawater mainly include dissolved oxygen content, salinity, carbonate, pH value, temperature, and flow rate (Ref 18).

The dissolved oxygen content is the most important factor affecting the corrosion of metals in seawater and is a depolarizer for metal corrosion in seawater. The higher the oxygen content in seawater is, the faster the corrosion rate of metals. As salinity increases, the conductivity of seawater increases, and the corrosion rate of metals in seawater increases. However, the increase in electrical conductivity in seawater leads to a decrease in the oxygen content in seawater, and the decrease in oxygen content reduces the oxygen depolarization effect of metals in seawater. Carbonation saturation is generally saturated under the pH value of seawater, and it is easily deposited on the metal surface to form a protective layer. When cathodic protection is applied, carbonate easily precipitates (Ref 19, 20). The effect of pH on corrosion varies from metal to metal. Generally, the stronger the acidity, the lower the pH value, and the greater the corrosivity, which is not conducive to the formation of a protective carbonate layer on the metal surface. Generally, the pH value of seawater is between 7.5 and 8.6, and the increase in seawater pH value

inhibits the corrosion of steel by seawater. The effect of seawater pH is much less than that of oxygen content on metal corrosion.

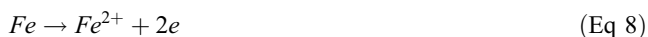
The general effect of increasing seawater temperature accelerates metal corrosion reactions. From kinetic analysis, it can be seen that the increase in seawater temperature accelerates the reaction speeds of the cathodic and anodic processes by which metals corrode in seawater, thereby accelerating the corrosion rate.

The corrosion of most metals in seawater is controlled by the oxygen depolarization reaction, which is mainly controlled by the diffusion of oxygen to the cathode surface. The flow rate of seawater can change the oxygen supply conditions, thereby affecting the corrosion of metals in seawater. When the seawater flow rate is slow, the corrosion of metals in seawater is mainly electrochemical corrosion. For metals that cannot be passivated in seawater, with increasing seawater flow rate, the corrosion rate of the metal increases. When the seawater flow rate exceeds a certain critical value, the seawater flow rate is faster, more solid particles are suspended in seawater, and the seawater has a greater effect on the metal. When seawater moves in a high-speed zone, the mechanical impact on the metal surface is very strong, the metal undergoes cavitation corrosion (Ref 21-24).

2.3.2 Electrochemical Corrosion. Steel for ship ballast tanks is generally required to have high comprehensive performance, weldability and good resistance to seawater, sea mud, and marine atmospheric corrosion (Ref 25). According to the “Code for Classification and Construction of Sea-going Steel Ships” (2018), the steel used for ballast tanks is generally grade A hull structural steel, and its chemical composition and mechanical properties corrode spontaneously in seawater. The corrosion of metals in seawater is mainly electrochemical corrosion. Since seawater is a typical electrolyte, the basic rules of electrochemical corrosion are applicable to seawater corrosion.

The electrochemical reactions of metals in seawater environments are as follows.

Anodic reaction:



Cathodic reaction:

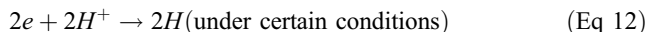
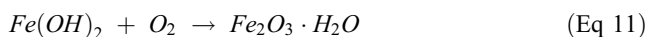


Figure 3 shows a schematic diagram of a short-circuit galvanic cell where steel corrodes in seawater.

In summary, when inert flue gas is introduced into the ballast tank, nitrogen can remove the dissolved oxygen in the ballast water, thereby reducing cathodic oxygen depolarization corrosion, that is, oxygen absorption corrosion, and reducing metal corrosion in seawater. However, when the introduced carbon dioxide dissolves in seawater and combines with water, it forms carbonates and bicarbonate ions, which reduce the pH value of seawater, aggravate the process of cathodic hydrogen depolarization, and is not conducive to the formation of

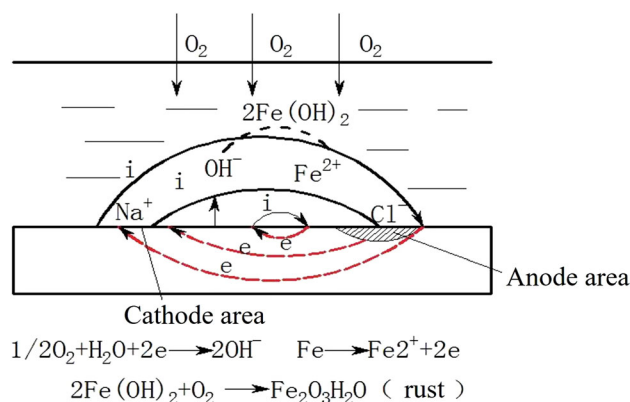


Fig. 3 Schematic diagram of a short-circuit galvanic cell corroding in seawater

protective properties on the metal surface. Carbonate layers and carbonate deposits precipitate out of solution, which in turn increases metal corrosion in seawater (Ref 26).

2.3.3 Methods for Analysis of Corrosion Samples. For the study of metal corrosion in this experiment, the corrosion degree is to study its corrosion behavior from the aspects of corrosion rate, surface analysis and electrochemical analysis.

- (1) Weightlessness method. After the sample was removed from the corrosive medium, the loose corrosion products on the surface were cleaned with water immediately, rinsed in clean water, wiped dry, wiped with anhydrous alcohol, air dried and weighed. According to the quality difference of the sample before and after corrosion, the average corrosion rate of the metal before and after corrosion in the corrosive medium is calculated (Ref 27).
- (2) Surface analysis. The surface analysis method adopts macroscopic morphology and microscopic morphology observation. The macro-morphology is captured by a digital camera to directly reflect the development process of corrosion area and rust layer on the specimen surface. Scanning electron microscope (SEM) is used to observe the morphology of corrosion products on the surface of corroded samples in different corrosive media, analyze the corrosion mechanism, and analyze the corrosion degree of corroded samples.
- (3) Electrochemical analysis. The standard three-electrode system was adopted in the electrochemical test. The corrosion sample after corrosion by different corrosive media was the working electrode, the auxiliary electrode—high-purity platinum sheet, and the reference electrode saturated calomel electrode (SCE). Electrochemical test includes open-circuit potential, polarization curve test. The potential-time curve of the open-circuit potential test, that is, the curve of the potential of the working electrode relative to the reference electrode changing over time, is used to detect the self-corrosion potential of the sample in different corrosive media. It is an important thermodynamic parameter for the corrosion of metal electrodes and can be used to judge the corrosion tendency of metals (Ref 28). The polarization signal applied by this method is weak and has little influence on the surface state of the sample (Ref 29).

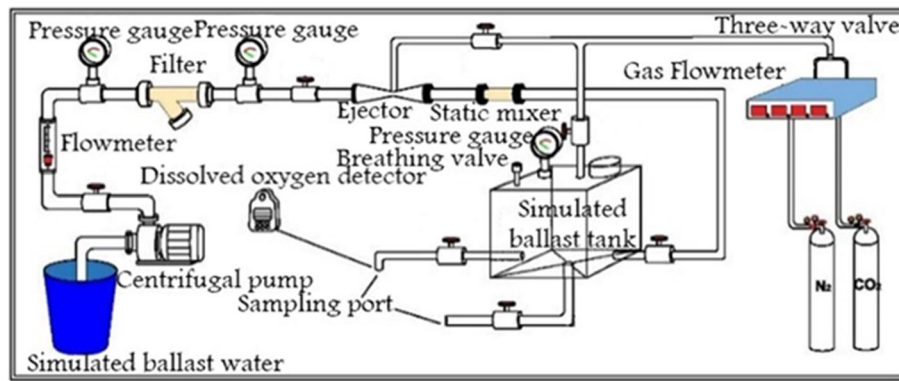


Fig. 4 Schematic diagram of the experimental system

3. Construction of an Experimental System for Ballast Water Treatment with Inert Flue Gas

An experimental system for inert flue gas carrier water treatment was established in the laboratory under normal temperature and pressure, as shown in Fig. 4. During the experiment, the irrigation volume was 100 L. High-purity N₂ and CO₂ were used to simulate inert flue gas, and the gas flow was adjusted by a mass flow controller. The simulated ballast water pumping device adopted a horizontal centrifugal pump with a rated flow of 1.5 m³/h. The ejector mixed the simulated inert flue gas and simulated ballast water (Ref 30) to form a high-pressure water flow, and the inert flue gas formed a cavity in the water flow. Under this action, it rose and overflowed the water surface and led to the atmosphere, which changed the ballast water environment. The function of the breathing valve on the simulated ballast tank was to maintain a slight positive pressure in the ballast tank when the inert flue gas and seawater mixed into the ballast tank to ensure that at this pressure, the partial pressure of the inert flue gas was greater than the dissolved oxygen in the ballast water and that the dissolved oxygen in the ballast water overflowed.

3.1 Experimental Simulated Seawater Configuration

The simulated seawater in the experiment was configured according to the formula of Mocledon artificial seawater. The temperature was 18-25 °C, the salinity was 25.5-35.5 PSU, and the pH value was 8.39 ± 0.27. The content of each component is shown in Table 1.

3.2 Selection of Test Algal Species and Bacteria

According to the International Maritime Organization (IMO) G8 guideline on the discharge of ballast water from ships, "In the treated ballast water, there are less than 10 viable organisms per cubic meter of ballast water with a minimum size greater than or equal to 50 μm/mL. The minimum size of viable organisms in ballast water is less than 50 μm but greater than or equal to 10 μm should be less than 10 per milliliter. Indicator microorganisms *Vibrio cholerae*, *Escherichia coli* and *Enterococcus* should be less than 1, 250 and 100 cfu/100 mL, respectively" (Ref 31). The algal species used in the test were selected from *Chlorella*. *Chlorella* is a common algal species in the sea. The size of common *Chlorella* is approximately 8 μm. It has the advantages of fast reproduction and easy cultivation

Table 1 Artificial seawater formula

Name	Molecular formula	Content, g/L
Sodium chloride	NaCl	26.726
Magnesium chloride	MgCl ₂ ·6H ₂ O	2.260
Magnesium sulfate	MgSO ₄ ·7H ₂ O	3.248
Calcium chloride	CaCl ₂	1.153
Sodium bicarbonate	NaHCO ₃	0.198
Potassium chloride	KCl	0.721
Sodium bromide	NaBr	0.058
Boric acid	H ₃ BO ₃	0.058
Sodium silicate	Na ₂ SiO ₃	0.0024
Sodium silicate	Na ₂ Si ₄ O ₉	0.0015
Phosphoric acid	H ₃ PO ₄	0.002
Aluminum hexachloride	Al ₂ Cl ₆	0.013
Ammonia	NH ₃	0.002
Lithium nitrate	LiNO ₃	0.0013

Table 2 1 L of chlorella stock solution medium formula

Name	Content
Sodium nitrate	75 mg
Sodium dihydrogen phosphate dihydrate	5.65 mg
Liquid metal	1.0 ml
Vitamin liquid	1.0 ml
Sodium silicate	50 mg
Pure water	1000 ml

in the laboratory. It has become a widely used in tests. *Escherichia coli* was selected as the test strain.

3.3 Test Algae and Bacterial Culture

The medium formulation of 1 L of *Chlorella* stock solution is shown in Table 2. The total culture time of *Chlorella* was 6 days, during which the changes in *Chlorella* were observed as shown in Fig. 5. *Escherichia coli* was cultured using LB medium, and its medium formula is shown in Table 3.

3.4 Flue Gas Simulation System

Systems that provide simulated flue gas include N₂ and CO₂ generators and mass flow controllers. The parameters of each gas are as follows: high-purity nitrogen, N₂ ≥ 99.999%, filling pressure 12.5 ± 0.5 MPa (20 °C); carbon dioxide, CO₂ ≥ 99.9%, filling pressure 12.5 ± 0.5 MPa (20 °C). The

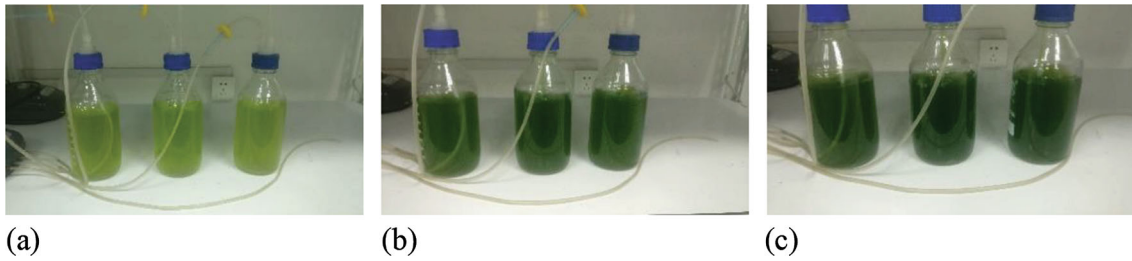


Fig. 5 Cultivation process of Chlorella (a) Day 1; (b) Day 3; (c) Day 5

Table 3 LB medium formula

Name	Content
Tryptone	10 g/L
Yeast extract	5 g/L
NaCl	10 g/L
Water	1000 mL

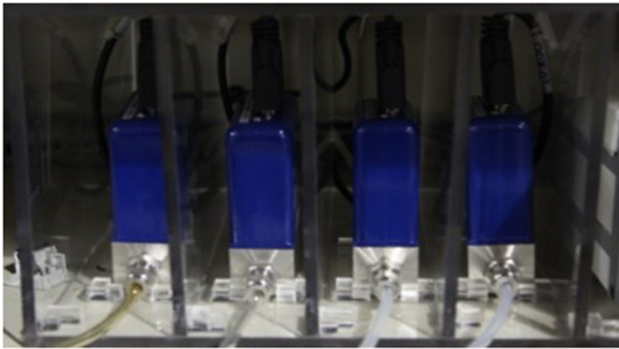


Fig. 6 Physical graph of the mass flow controller

corresponding flue gas simulation system is shown in Fig. 4, and the physical diagram of the mass flow controller and the mass flow controller adjustment display device is shown in Fig. 6. In the experiment, the volume flow rate of nitrogen, carbon dioxide and the mixture of nitrogen and carbon dioxide was 0.5 L/min, and the volume flow ratio was 7:1.

4. Experimental Results and Analysis

4.1 Analysis of the Effect of an Inert Flue Gas N_2 and CO_2 Mixture on Microbial Lethality

In the experiment, the supply volume ratio of N_2 and CO_2 was 7:1, the volume flow rate of N_2 was 437.5 mL/min, and the volume flow rate of CO_2 was 62.5 mL/min. The relationships between microbial lethality in ballast water and pH and dissolved oxygen concentration were studied, as shown in Fig. 7.

By fitting the test data, regression equations of dissolved oxygen and microbial lethality at different pH values were obtained, as shown in Table 4.

It can be seen from Fig. 7 that when the dissolved oxygen in the ballast water was constant and the pH value was equal to 6, the microbial lethality was the best. When the pH value was

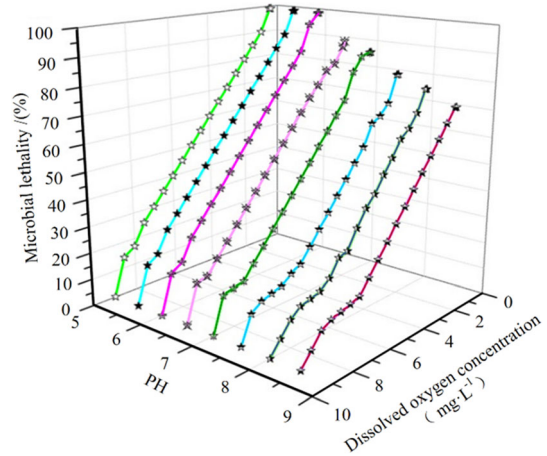


Fig. 7 Relationship between microbial lethality and pH and dissolved oxygen

less than 6, the microbial lethality remained basically unchanged. When the pH value was constant, as the concentration of dissolved oxygen in the ballast water decreased, the lethality rate of microorganisms increased. When the concentration of dissolved oxygen reached 0.5 mg/L, under the test conditions, the lethality rate of microorganisms was the best. Therefore, under the test conditions, when the pH value was 6 and the dissolved oxygen concentration was 0.5 mg/L, the microbial lethality was the highest. At this time, continuing to reduce the pH value had little effect on the lethality of microorganisms and remained basically unchanged.

Figure 8 shows the relationship between the survival rate of microorganisms in ballast water as a function of time during the 265 h test period.

The experimental data were fitted, and the regression equations of microbial lethality and time were obtained as shown in Eq 13, 14, 15, and 16, respectively, and the adjusted R-squared values of the curves were 0.999, 0.997, 0.96, and 0.95.

$$y = 100.75 - \frac{100.71}{1 + (x/28.39)^{2.59}} \quad (\text{Eq 13})$$

where x is time/h and y is the lethality rate of Chlorella in the experimental group/%.

$$y = 101.04 - \frac{101.39}{1 + (x/43.92)^{2.64}} \quad (\text{Eq 14})$$

where x is time/h and y is the lethality rate of Escherichia coli in the experimental group/%.

Table 4 Regression models of dissolved oxygen and microbial lethality at different pH values

pH	Regression equation	Correlation coefficient R^2
$5 \leq \text{pH} < 5.5$	$y = 8008.18 - 1588.53 \times \text{Ln}(x + 144.96)$	> 0.99
$5.5 \leq \text{pH} < 6$	$y = 7421.59 - 1493.32 \times \text{Ln}(x + 134.33)$	> 0.99
$6 \leq \text{pH} < 6.5$	$y = 8008.18 - 1588.53 \times \text{Ln}(x + 144.96)$	> 0.99
$6.5 \leq \text{pH} < 7$	$y = 8061.54 - 1575.83 \times \text{Ln}(x + 157.01)$	> 0.99
$7 \leq \text{pH} < 7.5$	$y = 1082.76 - 303.34 \times \text{Ln}(x + 26.10)$	> 0.99
$7.5 \leq \text{pH} < 8$	$y = 244.20 - 89.11 \times \text{Ln}(x + 5.94)$	> 0.99
$8 \leq \text{pH} < 8.5$	$y = 247.18 - 90.32 \times \text{Ln}(x + 6.25)$	> 0.99
$8.5 \leq \text{pH} < 9$	$y = 224.82 - 82.87 \times \text{Ln}(x + 5.92)$	> 0.99

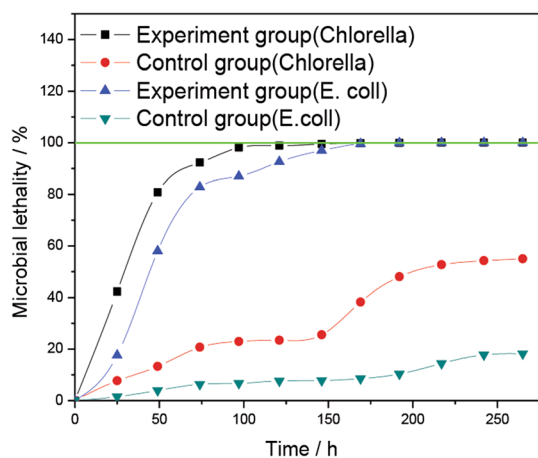


Fig. 8 Relationship between microbial lethality and time

$$y = 1.37 - \frac{0.22 \times [\exp(-5.59 \times 10^{-5}x) - 1]}{5.59 \times 10^{-5}} \quad (\text{Eq 15})$$

where x is time/h and y is the lethality rate of *Chlorella* in the control group/%.

$$y = 1.19 + \frac{0.038 \times [\exp(0.0038x) - 1]}{0.0038} \quad (\text{Eq 16})$$

where x is time/h and y is the lethality rate of *Escherichia coli* in the control group/%.

Figure 8 shows that at 100 h, almost all *Chlorella* were dead, and at 175 h, almost all *Escherichia coli* were dead, and no regeneration occurred in the subsequent time. The lethality rate of *Chlorella* in the treatment cabin was 100%, and the lethality rate of *Escherichia coli* was 99.98%, which was significantly greater than that of the control cabin. The content of *Escherichia coli* after treatment was 2.4 cfu/ml, which met the D-2 standard.

4.2 Analysis of Corrosion Weight Loss of Ballast Tank Steel Plate Specimens in Different Corrosive Media

According to the “Metal Materials Laboratory Uniform Corrosion Full Immersion Test Method” (GB 10124-88) standard, the size of the sample used for weight loss analysis was $50 \times 25 \times 3$ mm, and the size of the sample used for micro-morphology analysis and electrochemical morphology analysis was $10 \text{ mm} \times 10 \text{ mm} \times 3$ mm. Four kinds of corrosive media were configured: simulated seawater, the DO

concentration 0.5 mg/L in the corrosive media, pH = 6 in the corrosive media, the DO concentration 0.5 mg/L and pH = 6 in the corrosive media. For each medium, three sets of experiments were performed.

In this experiment, the average corrosion rates of the samples immersed in different corrosive media for 792 h was measured by the weight loss method are shown in Table 5, where m_1 is the mass of the sample before immersion, m_2 is the mass of the sample after immersion, and v_a is the average corrosion rate of the sample.

It can be seen from the test results in Table 5 that the average corrosion rate of the sample in the corrosive medium with a dissolved oxygen concentration of 0.5 mg/L was the lowest, and the average corrosion rate of the sample in the corrosive medium with a pH value of 6 was the highest. The average corrosion rate of the sample for the dissolved oxygen concentration of 0.5 mg/L was 85.84% slower than the average corrosion rate in the simulated seawater. Compared to the average corrosion rate of the sample in simulated seawater, the average corrosion rate of the sample in the corrosion medium with pH value of 6 increased by 44.24%. And the average corrosion rate of the samples in the corrosion medium with dissolved oxygen concentration of 0.5 mg/L and pH value of 6 decreased by 69.02% compared with the average corrosion rate of the sample in simulated seawater.

In summary, the main reason may be that the corrosion of metals in seawater is mainly controlled by oxygen depolarization corrosion. If the oxygen in seawater is completely removed, the metal will not corrode. Therefore, when the dissolved oxygen concentration was 0.5 mg/L, the average corrosion rate of the samples in the corrosive medium was the lowest. The pH value of seawater mainly affects the deposition of calcareous scale on the metal surface, thereby affecting the corrosion of metals in seawater. This calcareous layer formed on the metal surface has a relatively high resistance, which hinders the diffusion of oxygen to the cathode surface, reducing the effective cathode corrosion area and thereby inhibiting metal corrosion. In a corrosive medium with a pH value of 6, the pH value of seawater is reduced, affecting the deposition of calcium scale. Furthermore, the pH value decreases, H^+ increases, and hydrogen depolarization corrosion accelerates, so the average corrosion rate increases compared to that of simulated seawater. However, the test results show that the corrosion rate of the sample in the corrosion medium with dissolved oxygen concentration of 0.5 mg/L and pH value 6 is less than that of the sample in the simulated seawater corrosion medium. Although hydrogen depolarization corrosion is accelerated, the overall average corrosion rate is slower than that in

Table 5 Corrosion weight loss measurement results of samples immersed in immersed for 792 h in different corrosive media

		Length, mm	Width, mm	Thickness, mm	m_1 , g	m_2 , g	Weight loss, g	v, mm/a	v_a , mm/a
Simulated seawater	1#	49.95	24.92	2.87	26.918	26.667	0.251	0.121	0.113
	2#	49.95	24.91	2.84	27.296	27.141	0.155	0.075	
	3#	49.98	24.87	2.93	27.457	27.164	0.293	0.142	
DO concentration 0.5 mg/L	1#	49.95	24.86	2.92	28.118	28.081	0.037	0.018	0.016
	2#	49.96	24.94	2.91	27.786	27.757	0.029	0.014	
	3#	49.98	24.95	2.95	28.363	28.331	0.032	0.015	
pH = 6	1#	49.94	24.86	2.92	28.118	27.581	0.537	0.259	0.163
	2#	49.96	24.94	2.86	27.786	27.547	0.239	0.115	
	3#	49.98	24.88	2.95	28.363	28.128	0.235	0.113	
DO concentration 0.5 mg/L, pH = 6	1#	49.97	24.92	2.89	26.718	26.643	0.075	0.036	0.035
	2#	49.96	24.94	2.86	27.076	27.005	0.071	0.034	
	3#	49.95	24.87	2.93	27.387	27.294	0.073	0.035	

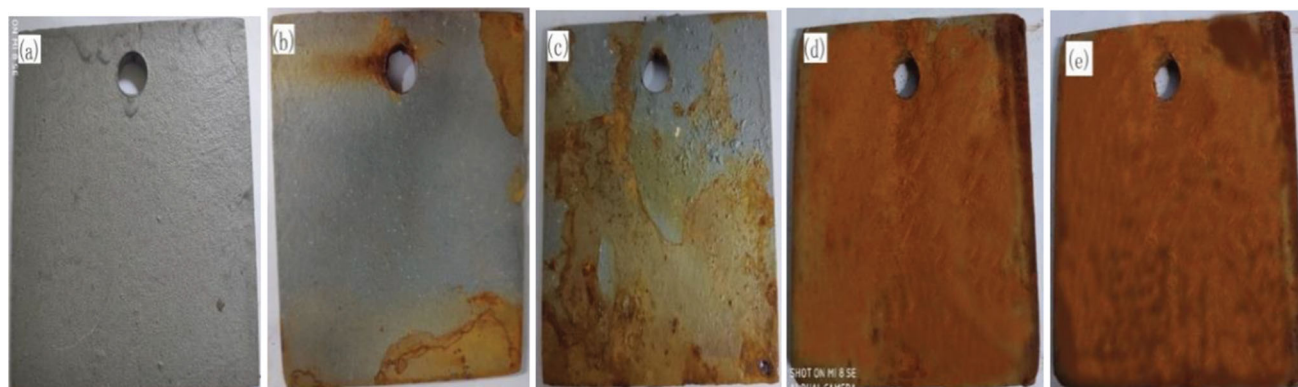


Fig. 9 Macroscopic surface morphologies of samples after immersion and corrosion in different corrosive media (a) Uncorroded sample (b) Sample immersed in corrosive medium with DO concentration 0.5 mg/L, (c) sample immersed in corrosive medium with DO concentration 0.5 mg/L and pH 6, (d) sample immersed in simulated seawater, and (e). Sample immersed in corrosive medium with pH 6)

the simulated seawater. Therefore, the corrosion rate of the sample in the corrosion medium with dissolved oxygen concentration of 0.5 mg/L and pH value 6 is slower than that in the original simulated seawater corrosion medium.

4.3 Analysis of Macroscopic Morphology Results of Ballast Tank Steel Plate Specimens in Different Corrosive Media

The macroscopic morphologies of the surfaces of the samples after being etched during full immersion in different corrosive media are shown in Fig. 9. Figure 9(a) shows the uncorroded sample.

After the samples corroded in different corrosive media, the surface state was basically uniform. It can be seen from Fig. 9(b) that for the samples in the corrosive media with a dissolved oxygen concentration of 0.5 mg/L, compared with the uncorroded samples, light yellow–brown corrosion appeared in some areas of the surface. Compared with the literature (Ref 19), the sample was in the initial stage of corrosion in this corrosive medium. Therefore, reducing the dissolved oxygen concentration in seawater can greatly reduce the corrosion of metals. From Fig. 9(c), it can be seen that in the corrosive medium with dissolved oxygen concentration of 0.5 mg/L and pH 6, compared with the sample in the corrosive medium with a dissolved oxygen concentration of 0.5 mg/L, the yellow color on the surface of the sample and the coverage area of brown spots increased. The

reason for this phenomenon may be that compared with the corrosive medium with dissolved oxygen concentration of 0.5 mg/L, hydrogen evolution corrosion and oxygen absorption corrosion occur in acidic solution, which increases hydrogen depolarization corrosion. It can be seen from Fig. 9(d) that in the corrosive medium simulating seawater, the surface of the sample was uniformly corroded, the rust layer was thick, the corrosion products showed red, brown and black inclusions, and the surface of the rust layer was loose. From Fig. 9(e), it can be seen that in the corrosive medium with pH 6, the rust layer on the surface of the sample was thicker than that of the sample in the original simulated seawater compared with the sample in the simulated seawater corrosive medium, which may be because the pH of seawater decreased, aggravating the cathodic hydrogen depolarization corrosion of metals in seawater. It can be seen from the observation results of the corrosion macroscopic morphology of the samples that the trend of the corrosion results and the results calculated by the weight loss method were consistent.

4.4 Analysis of Micromorphology of Ballast Tank Steel Plate Specimens after Immersion in Different Corrosive Media

To observe the corrosion of the samples after immersion in different corrosive media, the corrosion products were removed from the samples, and then the microscopic morphology was observed. The results are shown in Fig. 10.

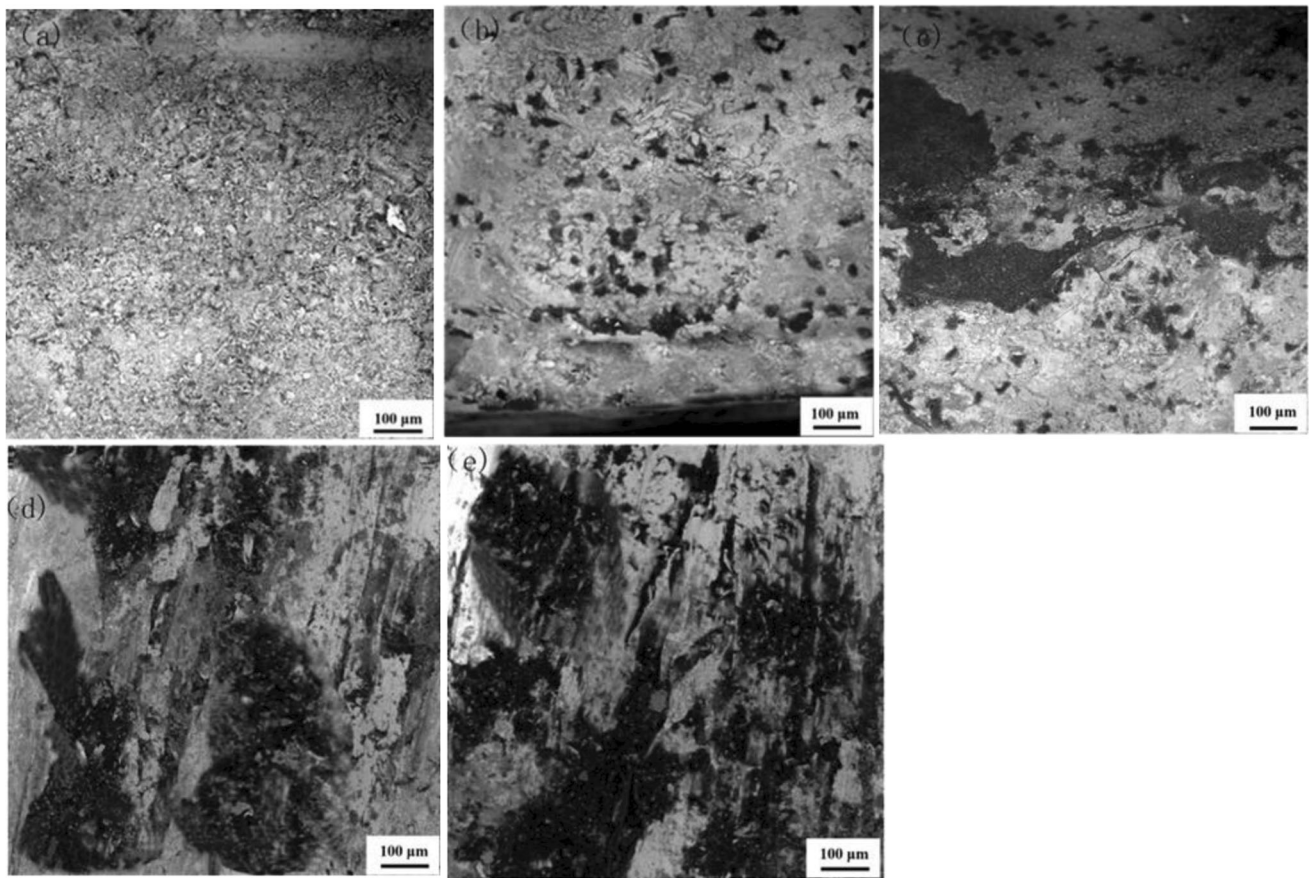


Fig. 10 Surface topography of the sample after corrosion after full immersion in different corrosive media (a). Uncorroded sample, (b) sample immersed in corrosive medium with DO concentration 0.5 mg/L, (c) sample immersed in corrosive medium with DO concentration 0.5 mg/L and pH 6, (d) sample immersed in simulated seawater, and (e) sample immersed in corrosive medium with pH 6)

Figure 10 shows the morphologies of carbon steel in different corrosion states. In Figure 10(a), the rust layer did not completely cover the metal, the surface was flat (Ref 32), a small number of small pits were produced, and the silver metal matrix could be seen. This was due to the formation of a surface oxide or hydroxyl oxide at the initial stage of corrosion (Ref 33). As shown in Fig. 10(b), the degree of corrosion worsened, with a larger number of black corrosion pits. The silver-white metal matrix was damaged, and the surface oxide or hydroxyl oxide was transformed into a rust layer. This was the initial stage of comprehensive heterogeneous corrosion (Ref 34). In Fig. 10(c), large and shallow patchy corrosion pits were clustered, accompanied by micro-cracks that were distributed unevenly on the surface (Ref 35). This was due to the aggravation of pitting and further expansion of the corrosion surface of the rust layer (Ref 36, 37). In Fig. 10(d) and (e), the corrosion degree was much worse, and a large and thick severe rust layer appeared. From the middle of the sample to both sides of the sample, the rust layer was stratified and peeled from the substrate, some parts were raised, and the corrosion bubbled (Ref 38). A large gully formed between the whole rust layer and the matrix, which easily underwent layered peeling, and corrosion products accumulated on the surface, which could not lead to a bare metal matrix (Ref 39). The rust layer with accelerated corrosion showed little change in morphology and generally presented a loose shape with more cracks.

4.5 Analysis of Electrochemical Corrosion Results of Samples in Different Corrosive Media

The corrosion potential results for the samples immersed in the corrosive medium with dissolved oxygen concentration 0.5 mg/L and pH 6, simulated seawater and the corrosive medium with dissolved oxygen concentration 0.5 mg/L and pH 6 are shown in Fig. 11.

The experimental results show that the potentials of all the samples in different corrosive media shifted negatively at the beginning, and with increasing immersion time, the potentials became more positive and finally reached a stable value. The potential of the sample in the corrosive medium with pH 6 reached the most negative potential, -755 mV, compared with the other corrosive media. The most negative potential was -651 mV in the corrosive medium with dissolved oxygen content 0.5 mg/L. After the corrosion potentials of the samples in different corrosive media reached stable values, they still varied within a certain range.

In summary, the reason that the initial potential of the samples shifted negatively when they were put into different corrosive media was mainly because the surface of the metal was covered with a dense oxide film formed by passivation. Then, the reaction was inhibited, and the potential was relatively positive. Subsequently, due to the corrosivity of the corrosive medium, the oxide film was destroyed, the metal surface was gradually activated, the effective corrosion area increased, the anodic reaction changed from weak to strong,

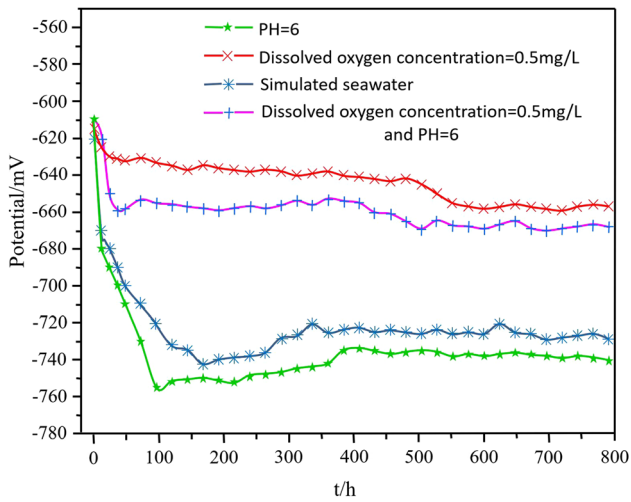


Fig. 11 Natural corrosion potential-time curves of samples in different corrosive media

and the potential changed from positive to negative (Ref 40). The potential reached the most negative value in the corrosive medium with pH 6, while the potential of the sample in the corrosive medium with dissolved oxygen concentration of 0.5 mg/L and pH 6 was relatively positive. As the immersion time continued to increase, the rust layer formed by the oxidation of the metal adhered to the surface of the material, the anodic reaction was blocked, and the potential shifted forward. Then, when a stable rust layer and an electric double layer formed on the metal surface, the potential began to stabilize; that is, during the entire 792 h corrosion period, with the extension of the immersion time, the open-circuit potential underwent a negative shift, and a positive process of moving to a stable state also reflected the change from destruction of the oxide film on the sample in the corrosive medium, to formation of the rust layer to stable adhesion of the rust layer. During the whole 792 h corrosion period, the open-circuit potential of the sample in the corrosion medium with dissolved oxygen concentration 0.5 mg/L and pH 6 did not change significantly. The stable potentials of different corrosive media were all less than their initial potentials. It can be seen from research results in the literature (Ref 25, 26, 41) that for steel materials, the more positive the corrosion potential is in the corrosive seawater medium, the better the corrosion resistance. Compared with the test results in this paper, it was concluded that the dissolved oxygen concentration of the sample with corrosion resistance at 0.5 mg/L was the best. Therefore, for the corrosion protection of metals, the removal of dissolved oxygen from seawater can be considered.

4.6 Polarization Curve Analysis of the Specimen in the Total Immersion Zone

During the corrosion process, the anodic and cathodic reaction rates were coupled on the electrode surface at a specific current density, and the polarization curve equation of the corroded metal electrode is shown in Eq 12. Potential polarization tests were performed on the samples immersed in different corrosive media. The polarization curves are shown in Fig. 12.

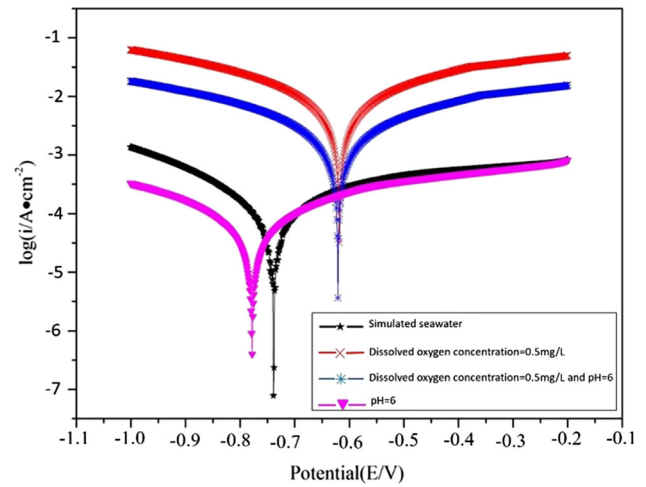


Fig. 12 Polarization curves of samples fully immersed in different corrosive media

$$I = I_{\text{corr}} \left\{ \exp \left[\frac{2.303(E - E_{\text{corr}})}{\beta a} \right] - \exp \left[-\frac{2.303(E - E_{\text{corr}})}{\beta c} \right] \right\}$$

Figure 12 shows that the polarization curve of the corrosion sample in the dissolved oxygen concentration of 0.5 mg/L was obviously shifted to the upper right, and the self-corrosion potential was shifted positively compared with the corrosion sample in the simulated seawater. The open-circuit potential test results were the same, and the corrosion tendency was reduced. The anodic polarization curve moved down significantly, and the slope decreased, indicating that the anode had an obvious polarization phenomenon, the metal dissolution reaction was blocked, and the corrosion reaction rate dropped rapidly. Compared with the polarization curve of the sample in the corrosive medium with pH = 6, the polarization curve slightly shifted to the left, the sample tended to be more severely corroded, and the corrosion rate increased slightly. Compared with the polarization curve of the sample in the corrosion medium with dissolved oxygen concentration 0.5 mg/L and pH = 6, the polarization curve slightly shifted to the left, and the corrosion rate was slightly increased. Therefore, under optimal conditions for microorganisms in ballast water, treating the ballast water with inert flue gas reduced the corrosion of ballast tanks.

5. Conclusions

- (1) The treatment of ballast water with inert flue gas N_2 reduced the dissolved oxygen in the ballast water, causing microorganisms to die due to the lack of oxygen necessary for growth. The volume ratio of inert flue gas N_2 and CO_2 was 7:1, the dissolved oxygen concentration in the ballast water was 0.5 mg/L, and the pH was 6. The mortality rate of *Chlorella* reached 100%, the mortality rate of *Escherichia coli* was 99.98%, and the microbial lethality met the D-2 standard.
- (2) The corrosion rate of the sample in ballast water treated with inert flue gas was experimentally studied. The aver-

age corrosion rate of the samples totally immersed in different corrosive media was measured by the weight loss method. The corrosion rate was the smallest in the corrosive medium with DO concentration 0.5 mg/L, and the corrosion rate was the largest in the corrosive medium with pH 6. The average corrosion rate of the sample in the corrosive medium with dissolved oxygen concentration 0.5 mg/L was 85.84% lower than that in the simulated seawater. The average corrosion rate of the sample in the corrosive medium with pH = 6 was compared with that of the sample in the simulated seawater increased by 44.24%. The average corrosion rate of the samples in the corrosive medium with dissolved oxygen concentration 0.5 mg/L and pH 6 decreased by 69.02% compared with the average corrosion rate of the samples in simulated seawater.

- (3) The electrochemical results for the samples in different corrosive media showed that the corrosion tendency of the samples in the corrosive media with DO concentration 0.5 mg/L was less than that in the simulated seawater. The corrosion tendency of the specimen in the corrosive medium with pH 6 was slightly greater than that of the specimen in the simulated seawater. The use of inert flue gas deoxidation to treat ship ballast water can reduce the corrosion rate of ballast tanks.

References

- D. Fan, *Analysis and Countermeasure Study of my country's Accession to Ballast Water Convention*, Dalian Maritime University, Dalian, 2013
- T.D. Waitel and J. Kazumil, *Practical Solutions for Ballast Water Treatment Hyde Marine Ballast Water Treatment Research*, University of Maryland, Maryland, 2009, p 8
- H. Zhang and B. Zhang, The Amendment to the Type Approval Guidelines of Ballast Water Management Convention and Associated Impact on the Implementation of the Convention, *China Marit. Saf.*, 2016, **01**, p 37–41
- S. Silva, T. Mardegan, and S.R.D. Araújo et al., Fabrication and Optical Properties of Strain-free Self-assembled Mesoscopic GaAs Structures, *Nanoscale Res. Lett.*, 2017, **12**(1), p 1–14
- S. Viitasalo and J. Rytkenen, Draft United Kingdom Type Approval Guideline for Ballast Water Management System, *Mar. Pollut. Bull.*, 2007, **2007**, p 57
- M.N. Tamburria, K. Wasson, and M. Matsuda, Ballast Water Deoxygenation Can Prevent Aquatic Introductions While Reducing Ship Corrosion, *Biol. Conserv.*, 2002, **103**, p 331–341
- T. McCollin, G.Q. Badia, K.D. Josefsen, M.E. Gill, E. Mesbahi, and C.L.J. Frid, Ship Board Testing of a Deoxygenation Ballast Water Treatment, *Mar. Pollut. Bull.*, 2007, **54**, p 1170–1178
- J. Xiao, K. Dang, Y. Song, and P. Yin, Study on Effect of Nitrogen Filled on Plankton in Ballast Water, *Mar. Environ. Sci.*, 2008, **05**, p 502–505
- Y. Zhou, Lu. Junbin, L. Zou, and M. Chen, Inert Gases for keeping Ecological Balance in Local Waters, *J. Shanghai Sci. Res. Inst. Shipp*, 2008, **31**(02), p 88–92
- Y. Ma, Application Study on Inert Gases Treatment of Ships' Ballast Water, *Chem. Def. Ships*, 2012, **02**, p 25–28
- D. Huang, Analysis on Venturi Oxygen Stripping of Ship's Ballast Water, *Mar. Technol.*, 2012, **06**, p 50–55
- P. McNulty, *Life Cycle Cost of the Venturi Oxygen Stripping Ballast Tank Corrosion Protection System in Double Hull Ships*, NEI Treatment Systems, Long Beach, 2007
- M.N. Tamburri and G.M. Ruiz, Evaluations of a Ballast Water Treatment to Prevent Aquatic Invasions and Ship Corrosion. *Paper presented at SNAME Maritime Technology Conference. October 19~21, Houston, TX* (2005)
- S. Tiku, *To Investigate the Effects of Using De-oxygenation as a Ballast Water Treatment System*, BMT Fleet Technology Limited, Kanata, 2006
- P. Cui, *The Corrosion Damage of Steel Structures of Harbor Projects*, Tianjin University, Tianjin, 2009, p 14–15
- X.A. Qi, Corrosion Environment of Mechanical and Electrical Products, *Modern Paint Finish.*, 2016, **19**(05), p 17–22
- Y. Lafontaine, Y. Chambers, S.P. Despatie, C. Gagnon, and C. Blaise, Effectiveness and Potential Environmental Impact of a Yeast-Based Deoxygenation Process for Treating Ship Ballast Waters, *Water Qual. Res. J. Can.*, 2011, **46**, p 55–75
- H. Li, Research on Corrosion Causes of Ship Ballast Tanks and Anti-corrosion Coatings, *China Water Transp*, 2010, **10**(01), p 26–27
- J. Wan, *Research on the Corrosion Behaviors and Mechanism of A517Gr Q Steel in Simulated Seawater*, Xi'an University of Technology, Xi'an, 2017, p 58–59
- D. Zhao, L. Li, Z. Li, and L. Yang, Research on Corrosion Behavior of Q235 Steel in Simulated Seawater Immersion Zone, *Hot Work. Technol.*, 2015, **44**(12), p 108–111
- G. Ding, Z. Yang, G. Huang, H. Yang, and K. Liu, Corrosion Potentials and Their Change Rules for Ferrous Metals in Natural Seawater, *Corros. Prot.*, 2018, **39**(02), p 99–102
- D. Zeng, B. Dong, and Z. Yu et al., Design of water-based annulus protection fluid for CO₂ flooding injection well, *J. Pet. Sci. Eng.*, 2021, **205**, p 108726
- D. Zeng, Z. Liu, and Y. Yi et al., Optimizing the performance of a composite corrosion/scale inhibitor for CO₂ flooding wells, *J. Natl. Gas Sci. Eng.*, 2022, **102**, p 104555
- B. Dong, D. Zeng, and Z. Yu et al., Corrosion Mechanism and Applicability Assessment of N80 and 9Cr Steels in CO₂ Auxiliary Steam Drive, *J. Mater. Eng. Perform.*, 2019, **28**, p 1030–1039
- J. Wu, D. Zhang, P. Wang, Y. Cheng, S. Sun, Y. Sun, and S. Chen, The influence of *Desulfovibrio* sp. and *Pseudoalteromonas* sp. on the corrosion of Q235 carbon steel in natural seawater, *Corros. Sci.*, 2016, **112**, p 552–562
- L. Zhang, S. Liu, Yu. Hongchuan Han, S.H. Zhou, C. He, and Q. Yan, Studies on the Formation Process and Anti-corrosion Performance of Polypyrrole Film Deposited on the Surface of Q235 Steel by an Electrochemical Method, *Surf. Coat. Technol.*, 2018, **341**, p 95–102
- JBT7901-2001, Uniform Corrosion Full Immersion Test Method for Metallic Materials in Laboratory
- C. Chunan and Z. Jianqing, *Introduction to Electrochemical Impedance Spectroscopy*, Science Press, Beijing, 2002, p 1–3
- H.J. Flitt and D.P. Schweinsberg, A Guide to Polarisation Curve Interpretation: Deconstruction of Experimental Curves Typical of the Fe/H₂O/H⁺/O₂, Corrosion System, *Corros. Sci.*, 2015, **47**(9), p 2125–2156
- M. Pecarevic, J. Mikus, I. Prusina, H. Juretic, A.B. Cetinic, and M. Brailo, New Role of Hydrocyclone in Ballast Water Treatment, *J. Clean. Prod.*, 2018, **188**, p 339–346
- S.F.C. Silva, T. Mardegan, S.R. Araújo, C.A.O. Ramirez, S. Kiravitaya, O.D.D. Couto, F. Iikawa, and C. Deneke, Fabrication and Optical Properties of Strain-free Self-assembled Mesoscopic Ga As Structures, *Nanoscale Res. Lett.*, 2017, **12**(1), p 1–14
- C. Wang, G.W. Cao, and C. Pan et al., Atmospheric Corrosion of Carbon Steel and Weathering Steel in Three Environments, *J. Chin. Soc. Corros. Prot.*, 2016, **36**(1), p 39–46
- Q. Yan, Q. Yin, and J. Cui, Effect of Temperature on Corrosion Behavior of E690 Steel in 3.5 wt.% NaCl Solution, *Mater. Res. Express*, 2021, **8**, p 01628
- W. Yueyi, Typical Corrosion Morphology of Metals, *Equip. Environ. Eng.*, 2006, **3**, p 31–37
- J. Xu, K.X. Wang, and C. Sun, The Effects of Sulfate Reducing Bacteria on Corrosion of Carbon Steel Q235 Under Simulated Disbonded Coating by Using Electrochemical Impedance Spectroscopy, *Corros. Sci.*, 2011, **53**, p 1554–1562
- J. Mu, Y.Z. Li, and X. Wang, Crevice Corrosion Behavior of X70 Steel in NaCl Solution with Different pH, *Corros. Sci.*, 2021, **182**, p 109310
- I.J. Jang, K.T. Kim, and Y.R. Yoo, Effects of Ultrasonic Amplitude on Electrochemical Properties During Cavitation of Carbon Steel in 3.5% NaCl Solution, *Corros. Sci. Technol.*, 2020, **19**, p 163–173

38. W.C. Jiao, H.B. Li, and J. Dai, Effect of Partial Replacement of Carbon by Nitrogen on Intergranular Corrosion Behavior of High Nitrogen Martensitic Stainless Steels, *J. Mater. Sci. Technol.*, 2019, **35**, p 2357–2364
39. T. Yuwan et al., Study on Corrosion Acceleration Behavior of Carbon Steel in Marine Atmosphere, *Compr. Corros. Control*, 2016, **30**(06), p 48–52
40. B. Dong, W. Liu, and L. Chen et al., Unraveling the Effect of Chloride Ion on the Corrosion Product Film of Cr-Ni-Containing Steel in Tropical Marine Atmospheric Environment, *Corros. Sci.*, 2022, **209**, p 110741
41. J.D. Wu, L.P. Guo, and Y.Z. Cao et al., Mechanical and Fiber/Matrix Interfacial Behavior of Ultra-High-Strength and High-Ductility Cemen-

titious Composites Incorporating Waste Glass Powder, *Cement Concr. Compos.*, 2022, **126**, p 104371

Publisher's Note Springer Nature remains neutral with regard to jurisdictional claims in published maps and institutional affiliations.

Springer Nature or its licensor (e.g. a society or other partner) holds exclusive rights to this article under a publishing agreement with the author(s) or other rightsholder(s); author self-archiving of the accepted manuscript version of this article is solely governed by the terms of such publishing agreement and applicable law.